A New Transient-Based Earth Fault Protection System for Unearthed Meshed Distribution Networks

J. D. Rios Penaloza, *Student Member, IEEE*, A. Borghetti, *Fellow, IEEE*, F. Napolitano, *Senior Member, IEEE*, F. Tossani, *Member, IEEE*, C. A. Nucci, *Fellow, IEEE*

Abstract— This paper deals with the protection against earth faults in medium voltage meshed networks with unearthed neutral. A communication-supported protection system is proposed and assessed through numerical simulations. The protection system is based on the use of directional relays installed at both ends of each line of the network. Each relay communicates by sending permissive signals following the so-called directional comparison overreaching transfer trip scheme. Each directional relay implements a new transient fault detection algorithm based on the angle between the zero-sequence voltage and current phasors. The phasors are estimated at the dominant frequency of the network transient-response within the first milliseconds after the fault, which range can be evaluated by means of a simplified circuit equivalent representation. The performances of the protection system and the detection algorithm are evaluated for different network configurations. By using a specifically developed co-simulation tool that interfaces EMTP-RV with Matlab, the influence of the communication latency is also analyzed. A Monte Carlo method is applied to analyze the effects of fault resistance, incidence angle and fault location variations. Results of a real-time simulation obtained in the Opal-RT environment further support the applicability of the algorithm.

Index Terms— Communication latency; Distribution network; Dominant transient frequency; Earth fault protection; Earth mode current; Earth mode voltage; EMTP; Operation zone; Power system faults.

I. Introduction

Medium Voltage (MV) networks are typically operated in radial configuration due to straightforward control, planning, and design of the protection schemes. However, due to the growing installation of Distributed Generation (DG), open ring configurations, typically used in urban power distribution systems, are being replaced in some cases by loop and meshed network configurations. As most power outages in distribution systems are due to faults, the meshed network configuration may improve the power quality with respect to the radial one [1]–[4] by reducing the duration and number of interruptions. Meshed configurations may also help to increase DG hosting capacity, operation flexibility, and voltage control, as well as to decrease power losses and maintenance efforts [5]–[7]. However, the protection scheme design is more complex than in radial networks, particularly for the case of compensated or unearthed neutral, in which the small values of the single-phase-to-ground fault currents reduce the sensitivity of directional earth fault protections based on the use of zero-sequence voltage and current phasors at the utility frequency.

This paper deals with the protection for these types of networks, namely MV meshed networks with unearthed neutral: the development of a communication-supported protection scheme based on the analysis of the fault-originated voltage and current transients is proposed to accomplish that.

Transient-based protective methods are considered a promising and efficient solution in unearthed and compensated networks, since they are not significantly affected either by the level of compensation of the neutral or by the fault characteristics [8], [9]. Furthermore, transient-based algorithms allow, in general, for a prompt operation. This is an important aspect especially in unearthed MV networks as an earth fault may lead to considerable overvoltages in the sound phase conductors. The overvoltages may cause a subsequent line-to-line fault or an earth fault in a different phase within a delay of, e.g., 160 ms [10]. Another requirement for a prompt relay operation is due to the presence of DG, since connection rules may require that generating units stop feeding the faulty area within a limited time interval (again, for instance, 160 ms, as in [11]). The presence of DG is deliberately disregarded in this paper, since its inclusion would require an extended and more specific analysis of the effects of harmonics and disconnection of some units, among other issues.

Different transient-based methods to detect the faulty section in MV unearthed and compensated neutral networks are documented in the literature. The algorithm presented in [12] evaluates the relation between the zero sequence voltage and the zero sequence charge, estimated as the integral of the zero sequence current. The fault detection techniques presented in [13]–[15] are instead based on the estimation of the earth-mode impedance that depends on the measure of the early time voltage and current earth modes and on the dominant transient frequency. The algorithm presented in [16] computes the zero sequence power factor estimated from active and reactive powers calculations. Most of these

algorithms are assessed in radial MV networks, and their application in a meshed network is not considered.

The typical aspects that might affect the performance of such transient methods are described in [9]:

- the line unbalance can reduce the performances of zero-sequence angle-based and zero-sequence energy-based indicators;
- faults at the zero-crossing voltage hamper the methods based on power, energy, and impedance calculations;
- the presence of underground cables negatively affects the current polarity-based and zero-sequence admittance-based indicators.

The transient-based protection algorithm presented in this paper implements some specific countermeasures to deal with the above-mentioned negative aspects. The directionality of the fault is determined by the phase angle displacement between the earth-mode voltage and the earth-mode current at the dominant transient frequency. The implementation of a Butterworth digital filter and a zero-padding process to the input signals enhances the accuracy of the estimation of the dominant frequency and the angle, even at low values of sampling frequency, attainable by modern relays. Relays are installed at both ends of each line. Each relay communicates to the relay at the opposite line end by exchanging permissive signals following the so-called directional comparison permissive overreaching transfer trip (POTT) scheme [17]. In this scheme, when the relay senses the fault within its protection zone it sends a permissive signal to the relay at the opposite end. Moreover, the relay outputs a trip signal when two conditions are met: i) it senses the fault within its protection zone and; ii) a signal is received from the relay at the opposite line end.

The protection performances are assessed for the case of different unbalanced MV meshed networks. One case study considers the presence of both overhead and underground lines. The Monte Carlo method is applied to analyze the influence of fault resistance, with typical values in unearthed distribution networks as reported in [10], incidence angle, and fault location variations.

The analysis of the adopted POTT scheme performance is accomplished taking into account a probability distribution of the delays of the spread spectrum radio communications between the relays in simulations performed by using the specifically developed interface between the ElectroMagnetic Transient Program (EMTP-RV) environment and Matlab [18]. A further test of the applicability of the approach has been carried out by using the Opal-RT real-time environment.

The paper is structured as follows. Section II presents the protection algorithm, the communication system, and the simulation tool used for the performance analysis. Section III presents the simulation cases and the results. Section IV discusses the results and concludes the paper.

II. THE TRANSIENT-BASED PROTECTION SYSTEM

The following subsections provide a theoretical background and describe the algorithm, the communication infrastructure needed by the protection system, and the simulation tool adopted for the analysis of the performances.

A. Theoretical background

When a single-phase-to-earth fault occurs in an unearthed neutral network, a transient phenomenon arises. Basically, the transient can be interpreted as composed by a component due to the lowering of the faulty phase conductor voltage and by a component due to the rising of the voltages in the sound phase conductors [13]. The frequencies of these two transient components vary in different ranges and have different amplitudes. Following [13]–[15], the latter component is adopted in the proposed fault detection algorithm, corresponding to the higher amplitude and the lower frequency with respect to the discharging one.

The analysis presented in [13], [14] for radial networks is extended for meshed ones. Directional relays detect zero-sequence current phasor at the dominant transient frequency i_0 and the corresponding voltage phasor v_0. In radial networks, relays of faulty feeders detect i_0 lagging v_0 while those of healthy feeders detect i_0 leading v_0, considering the positive direction of the current from the bus to the line. As illustrated in Fig. 1, in meshed networks, relays at both ends of faulty lines detect i_0 lagging v_0 likewise radial networks, but in healthy lines one of the relays can see i_0 lagging v_0 (see relay 1A in Fig. 1). The condition in which i_0 is leading v_0 can be seen by both relays at both ends of healthy lines or by only one of the two. The latter case may happen in lines of limited length where the leakage current through the line capacitance is small, therefore the currents at both ends of the line have similar magnitude and opposite direction.

Fig. 2 is the reduced equivalent circuit of the network, where the power system behind the faulty line is represented by means of Thevenin's equivalent generators and impedances at positive, negative and zero sequences, together with the transfer impedance needed in meshed networks [19]. In Fig. 2, $z_{line,1}^{(+\text{-}0)}$ and $z_{line,2}^{(+\text{-}0)}$ represent the sequence impedances of the faulty line, $z_1^{(+)}$, $c_1^{(0)}$, $z_2^{(+\text{-})}$ and $c_2^{(0)}$ are the positive and negative equivalent impedances and the zero capacitances
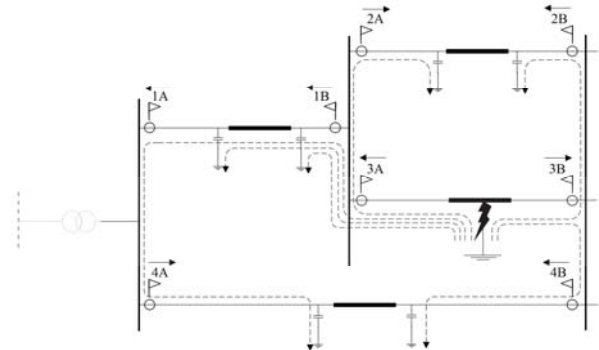

Fig. 1. Representation of the polarity of the phase displacement of zero sequence current respect to zero sequence voltage during an earth fault in a meshed network.
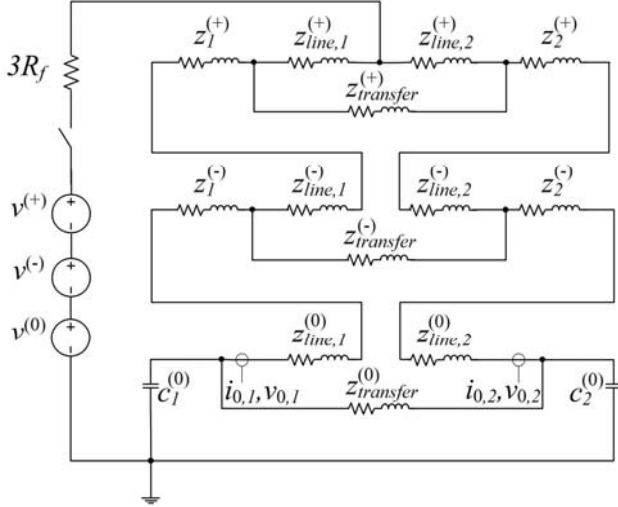
Fig. 2. Reduced equivalent circuit of the system in single-phase-to-ground fault condition.

seen from the two ends of the line, $v^{(+,-,0)}$ are the pre-fault sequence voltages and R_f is the fault resistance. The circuit can be further reduced into an RLC circuit which inductance and capacitance L_{eq} and C_{eq} provide the dominant frequency of the voltages and currents $v_{0,1}$, $v_{0,2}$, $i_{0,1}$ and $i_{0,2}$ measured by the relays at the ends of the faulted branch

$$f_{dom} = \frac{1}{2\pi\sqrt{L_{eq}C_{eq}}} \tag{1}$$

The application of the equivalent circuit for the evaluation of the transient frequency is illustrated in the next Sections.

B. The algorithm

The main steps of the proposed protection scheme are illustrated in Fig. 3.

The scheme is based on the estimation of the directionality of the fault, which is used to guarantee the security and dependability of the protection system in the meshed network. As earth-mode current i_0 could have very low values, particularly for high resistance faults, both current i_0 and corresponding voltage v_0 are monitored. If one of them exceeds a predefined threshold, which should be specified for each network, the algorithm starts the process to determine the directionality. Current and voltage earth modes i_0 and v_0 are estimated from the measurements of the phase quantities during time window t_{win}. Since the transient duration is affected by network parameters [9], the time window is chosen for each network depending on the expected range of transient frequencies, as it will be described next. A Butterworth bandpass digital filter and the Discrete Fourier Transform (DFT) are applied to i_0 to find the dominant transient frequency f_{dom} of the fault-originated transient. To obtain the results shown in this paper, the Fast Fourier Transform (FFT) of i_0 is calculated, by zero-padding the record in order to increase the frequency resolution [20]. Then, the phasors of both i_0 and v_0 at the dominant transient frequency are estimated and the angular displacement θ
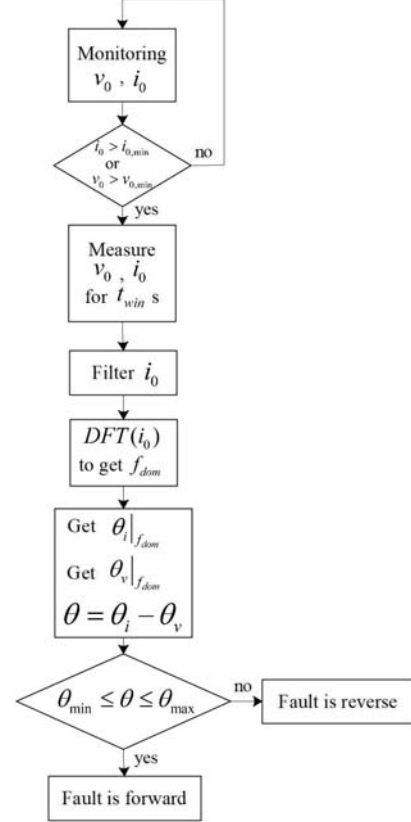

Fig. 3. Protection algorithm flowchart to determine the fault directionality.

between the phasors is used to define the directionality of the fault.

As illustrated in Fig. 4, if θ falls within the operation zone, defined by angles θ_{min} and θ_{max} (measured from the v_0 phasor angle that is taken as reference), the fault is declared as forward. Section III provides specific details of the procedure, particularly for the bandpass filter and minimum and maximum angle values, for each considered case study.

In the proposed algorithm, the estimation of the dominant frequency is of utmost importance to determine the directionality of the fault. A first evaluation of the expected range of these frequency values is obtained by using the equivalent circuit of Fig. 2. The knowledge of the range of values is useful for the application of the Butterworth bandpass filter and the DFT.
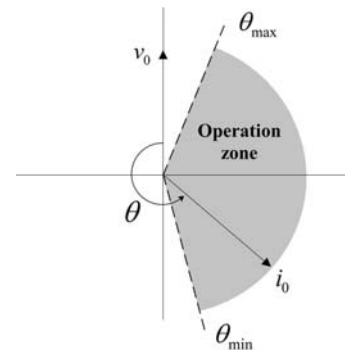

Fig. 4. Operation zone.

C. The communication system

The relays at both branch terminals exchange permissive signals to each other when they sense the fault in the forward direction. This can be considered as a directional comparison overreaching transfer trip scheme.

The adoption of a permissive scheme allows shorter operating times than blocking schemes [21], particularly when a transient earth fault protection is adopted. Indeed, in blocking schemes the coordination time, i.e., the minimum operating time for the protection, must be larger than the maximum expected latency of the blocking signal. This requirement is not needed in permissive schemes.

In typical communication systems, the average latency values is less than half cycle [21]. The speed of the communication channels depends on many factors: the data rate of the channel, the message packet size, and the equipment latency. While optic fibers are an attractive communication technology for the implementation of protective schemes due to the high bandwidth and communication speed, the installation costs could be prohibitive for the distribution system companies. Radio systems are a cheaper solution and are adequate for directional comparison schemes [17]. They do not require any right-of-way or physical conductor, but they need line-of-sight [21]–[23].

For the assessment of the communication-supported protection system, this paper considers a spread spectrum radio technology for the communication between stations. A typical latency between 4 and 5.6 ms is expected, depending on the channel data rate [21], [24]. For the tests, the truncated normal distribution of Fig. 5 is used to represent the latency, with mode equal to 5.6 ms. The standard deviation of the untruncated distribution is equal to 22 ms. The 99.9% of delays are lower than 67 ms, therefore the probability of exceeding the maximum end-to-end delay recommended in [25] is negligible.
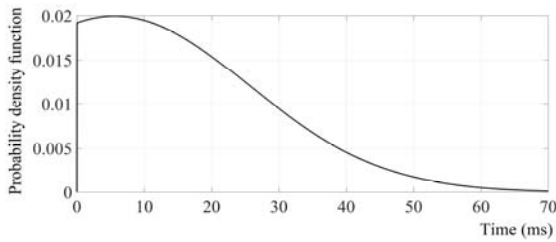

Fig. 5. Probability density function of time delays.

To account for the lag due to the relay information processing, a constant time delay is added, which considers: 0.8 ms for the analog filter, one sampling period to account for the maximum sampling latency, and the duration of the time window in which the measurements are taken for the digital filter. The relay's contact closing operation time, typically in the order of 10 µs [24], is neglected.

D. The simulation tools

The expected performances of the protection system are assessed by using a specifically developed co-simulation environment which interfaces EMTP-RV and Matlab, based on the procedure described in [26]. A virtual port allows the exchange of information between the two simulation environments at each step of the EMTP-RV time domain simulation. In EMTP-RV (*server*) the waveshapes of the power system currents and voltages in both phase and modal domain are calculated, while in Matlab (*client*) the communication-supported protection system is modeled. A Matlab script determines the directionality of the fault and emulates the sending of permissive signals for the breaker operations, considering communication delays and trip times.

As illustrated in Fig. 6, the virtual port is set up at the beginning of the simulation. When a fault occurs, EMTP-RV initiates to send information to Matlab at each time-step through a dynamic link library (DLL). Vice versa Matlab sends information when necessary to EMTP-RV. Time synchronization is done by exchanging specific flag signals and time stamp information at each time-step. When the Matlab routine completes its tasks, it closes the communication port with EMTP-RV, which then carries out the residual simulation process.
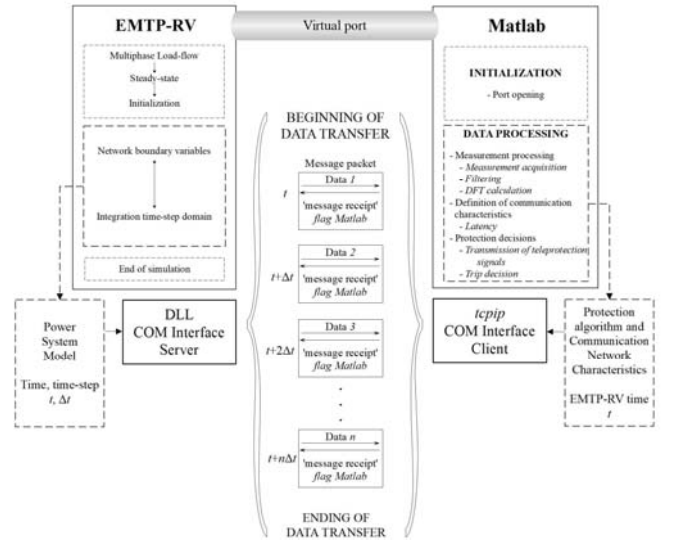

Fig. 6. Structure of the co-simulation environment that interfaces EMTP-RV with Matlab. The task division between both tools is illustrated.

III. Test Results

Three network cases are analyzed, denoted as *Case A*, *B* and *C*. *Case A* and *B* have the network topology shown in Fig. 7, which is a modified IEEE 14-bus test system with the line geometry of Fig. 9a, that is characterized by a significant asymmetry. In *Case A*, the lines are 3 km long, while in *Case B* they are 0.5 km long.

The network of *Case C* has the topology of the Cigré European MV distribution network benchmark [27] shown in
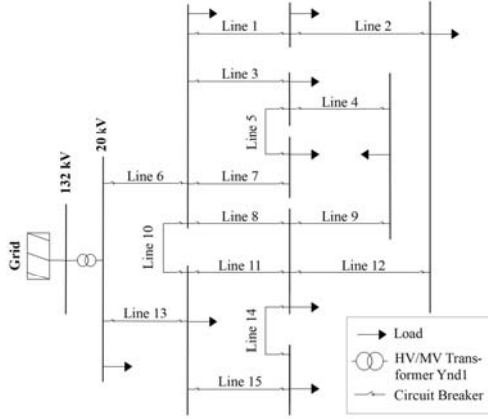
Fig. 7. Modified IEEE 14-bus test network. MV network for *Case A* and *B*.

Fig. 8. It is composed of two main feeders: one (denoted as Feeder A in Fig. 8) is composed by underground cables with the geometry of Fig. 9c, the other (Feeder B) is composed by overhead lines with the geometry of Fig. 9b.

The high voltage (HV) side of the transformers is wye-connected with the neutral solidly earthed, while the MV side is delta-connected. For the lines, a constant parameter model is used. For the simulations, a time step of 0.2 µs was used. For the relays, a sampling frequency f_s of 8 kHz is assumed, unless otherwise specified.

A. EMTP-Matlab test results

1) Case A

A preliminary analysis is carried out with the equivalent circuit of Fig. 2 described in Section II-A for a first estimation of the dominant transient frequencies. For such purpose, a sequence of faults is simulated in the middle of lines 2, 9 and 14 of the network of Fig. 7, with fault resistance varying between 0 and 100 Ω in steps of 5 Ω.

Fig. 10 shows the dominant transient frequencies estimated by using the equivalent circuit, together with the frequencies estimated by using the real network. The latter, considered as benchmark, show the reasonable accuracy of the results provided by the equivalent circuit. The results of Fig. 10 motivate the choice of a filter centered at 2.2 kHz (f_0). This is also supported by the similar results obtained by repeating the analysis for all the other lines. Indeed, one of the advantages of the use of an equivalent circuit is that several simulations can be carried out with very low computational effort. Moreover, on one hand the equivalent circuit does not take into account the wave propagation, thus it neglects reflections that influence the waveform, on the other hand, the transient in the equivalent circuit is less damped, thus it is easier to extract the dominant frequency. By using the equivalent circuit, the fault location is varied along each line as well as the fault incidence instant, uniformly distributed over the period corresponding to the utility frequency. Based on the results of the analysis, a filter bandwidth (*BW*) equal to 2.2 kHz is chosen.
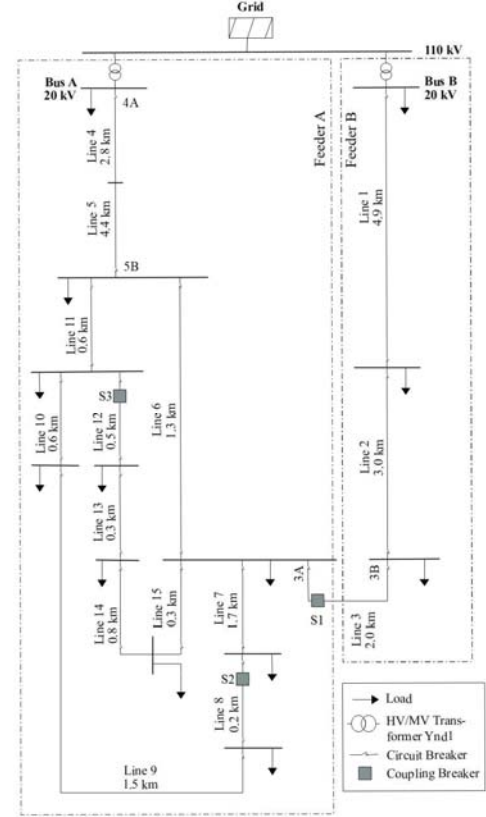

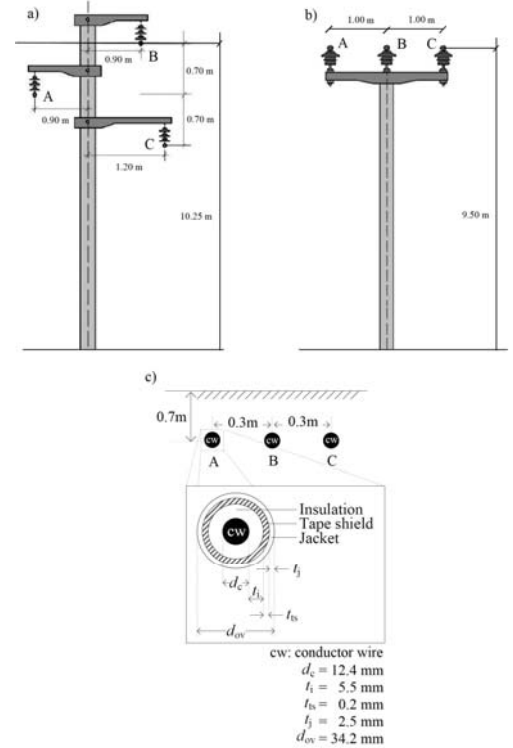Fig. 8. Cigré European MV distribution network benchmark for *Case C*.

Fig. 9. Distribution overhead line and cable geometries. a) Overhead line for *Cases A* and *B*. b) Overhead line for *Case C*. c) Cable for *Case C*, adapted from [27].
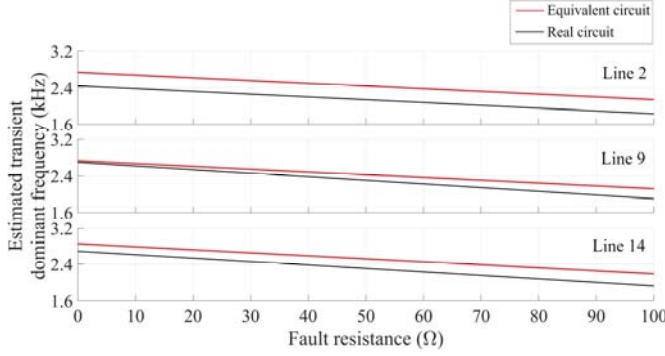
Fig. 10. Comparison between estimated transient dominant frequencies obtained with the real network and the equivalent circuit, for faults in different lines of the network of Fig. 7.

Due to the identified frequency range, a time window t_{win} of at least 1 ms is needed for the transient dominant frequency evaluation.

In order to illustrate the robustness of the algorithm in front of the chosen filter, in particular its center frequency value, Fig. 11 shows the dominant transient frequency and the estimated angle for different f_0 values. Fig. 11a shows the results for a relay in Line 9, i.e. the faulty line, and Fig. 11b for a relay in Line 8, i.e. a healthy line. For the healthy line the dominant transient frequency identified by the DFT is different when f_0 = 2.6 kHz. Fig. 11 shows that the estimated angles in both relays do not vary significantly around the dominant transient frequency and do not differ considerably for filters with different f_0 values. Moreover, the value of BW has a limited influence too. Analogous results are obtained for the other lines and fault locations.

To assess the influence of the zero-padding, we define the frequency step of the DFT as,

$$f_{step} = \frac{f_s}{L} \qquad (2)$$

where L is the length of the signal. Since f_s = 8 kHz and the time window is 1 ms, the acquired signal has a length of 9 points, thus f_{step} = 888.89 Hz. Such value is high for the considered f_0. Indeed, f_{step} is 40.4% of f_0. By zero-padding the length of the signal is increased to 64 points. For such length f_{step} = 125 Hz, i.e. 5.7% of f_0. The effect of the zero-padding for a particular case is illustrated in Fig. 12. The difference between the dominant transient frequencies estimated with and without the padding process is considerable.

As we mentioned, for a fault in the forward direction, the earth-mode current at the dominant transient frequency leads the earth-mode voltage by 270° [18]. Therefore, the maximum operation zone is between 180° and 360°. To decrease the probability of unnecessary trips, a reduced operation zone is identified. This selection is done by simulating 500 faults in three different lines, namely lines 2, 9 and 14 of Fig. 7, with different fault locations, fault incidence angles and fault resistances in the range between 0
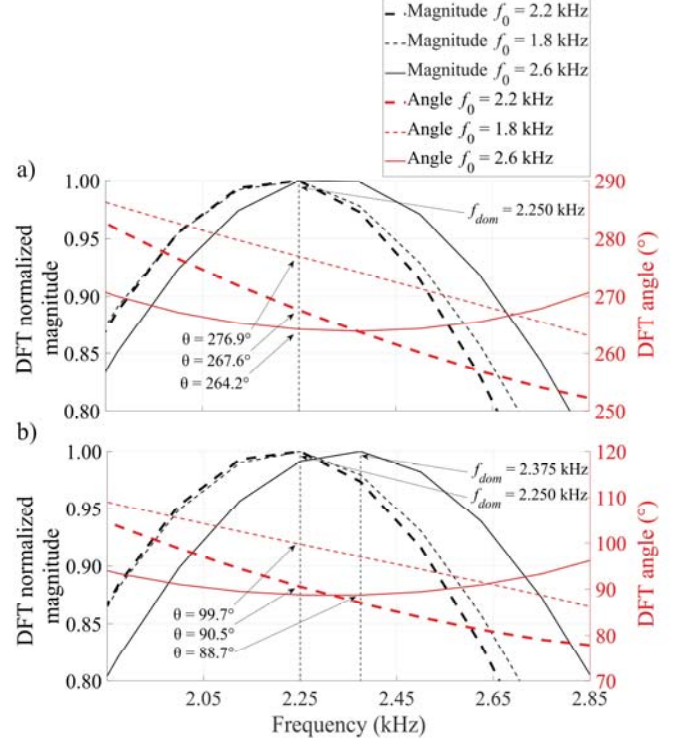

Fig. 11. DFT modulus and angle for different values of the filter center frequency f_0, estimated by relays at a) the faulty line and b) a healthy one. The DFT modulus is normalized.
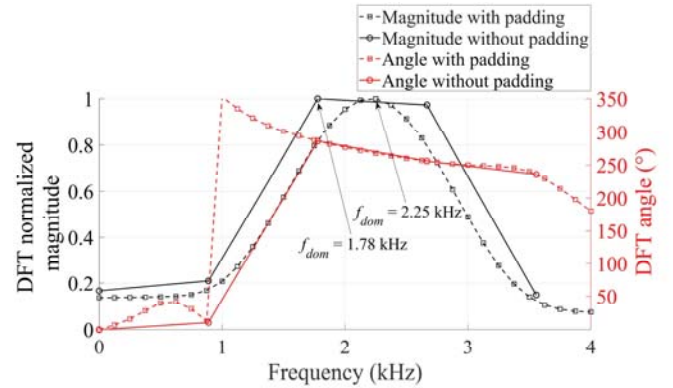
Fig. 12. DFT modulus and angle with and without zero-padding. The different values of f_{step} is evidenced by the distance between consecutive points (squares when the signal is padded, circles when it is not).

and 100 Ω. In Table I the obtained operation zone are reported, i.e. θ_{min} and θ_{max}, that maximizes the protection performance, for given filter characteristics and time window, in terms of expected rates of failures to trip and of unnecessary trips.

To further validate the effectiveness of the considered operation zone, a Monte Carlo analysis is carried out. A series of 2000 faults randomly distributed within the entire network are simulated, by varying the fault incidence angles over one power frequency period and the fault resistances between 0 and 100 Ω. The characteristics of the protection system are reported in Table I. The results show a 0.55%

failure to trip rate and a 0.5% unnecessary trip rate. The minimum peak values for v_0 and i_0 during the fault are 15.44 kV and 0.27 A, respectively.

TABLE I
PROTECTION ALGORITHM CHARACTERISTICS AND MAIN RESULTS FOR THE MV NETWORK OF FIG. 7 (*CASE A*)

Filter f_0/BW (kHz)	2.2/2.2		
t_{win} (ms)	1.0		
$\theta_{min} - \theta_{max}$	$220° - 350°$		
$v_{0,min}$ (kV)	1.5		
$i_{0,min}$ (A)	0.2		
Faulted line	**Line 2**	**Line 9**	**Line 14**
Failures to trip	0.00%	0.00%	0.00%
Unnecessary trips	0.40%	0.00%	1.40%

Different angle values modify the results, either enhancing security, by reducing the operation zone, or dependability by enlarging it. In Table II the results for different operation zones are summarized, obtained by varying the original angles by ±10°. The results obtained with a range between 180° and 360° is also reported.

TABLE II
MONTE CARLO RESULTS FOR DIFFERENT OPERATION ZONES (*CASE A*)

$\theta_{min} - \theta_{max}$	**Failures to trip**	**Unnecessary trips**
180° - 360°	0.10%	7.55%
220° - 350°	0.55%	0.50%
210° - 360°	0.15%	0.95%
230° - 340°	1.15%	0.25%

Fig. 13 shows the histogram of the operation times. The delay introduced by relay processing is considered equal to 1.93 ms (the time window is 1 ms). The protection algorithm operates mostly within three cycles from the fault initiation and does not exceed 100 ms even in the worst communication conditions.

2) Case B

As already mentioned, the network of Case B is the same as for *Case A*, but the lines are 0.5 km long instead of 3 km.
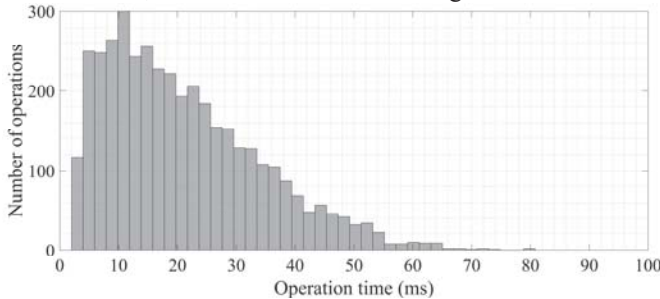

Fig. 13. Histogram of relay operation times for the network of Fig. 7 (*Case A*)

It can be seen from (1) that, for a specific network, shorter lines will result in both smaller equivalent capacitance and inductance, thus greater dominant frequencies. This is confirmed by the preliminary estimation of the dominant transient frequencies made by the equivalent circuit, which suggests the implementation of a filter centered at 7 kHz and

with a bandwidth of 4.5 kHz. To satisfy the criterion that the sampling frequency must be at least twice the highest frequency, a sampling frequency of 8 kHz is insufficient. For the sake of the protection algorithm validation, a sampling frequency of 25 kHz is therefore applied in this case.

A Monte Carlo analysis is carried out with the same characteristics as for Case A. The characteristics of the protection system and the results obtained for different operation zones are reported in Table III. The minimum peak values for v_0 and i_0 during the fault are 15.98 kV and 0.05 A, respectively. In this case, using a current threshold lower than 0.05 A could result into a too sensitive protection. Hence, we use a higher value since the voltage threshold will activate the algorithm when the current is very low.

TABLE III
PROTECTION ALGORITHM CHARACTERISTICS AND MAIN RESULTS FOR THE MV NETWORK OF FIG. 7 (*CASE B*)

Filter f_0/BW (kHz)	7.0/4.5	
t_{win} (ms)	0.5	
$v_{0,min}$ (kV)	1.5	
$i_{0,min}$ (A)	0.2	
$\theta_{min} - \theta_{max}$	**Failures to trip**	**Unnecessary trips**
180° - 360°	2.45%	13.60%
220° - 345°	5.95%	3.00%
210° - 355°	4.90%	6.85%
230° - 335°	7.60%	1.20%

As shown by the results of *Case B*, the low values of capacitance of networks with short lines lead to higher frequencies and make it difficult for the protection algorithm to estimate the dominant transient frequency and the angle, compromising correct operation.

Fig. 14 shows the histogram of the operation times. The delay introduced by relay processing is considered equal to 1.34 ms, as the time window used is 0.5 ms and the sampling frequency is 25 kHz.
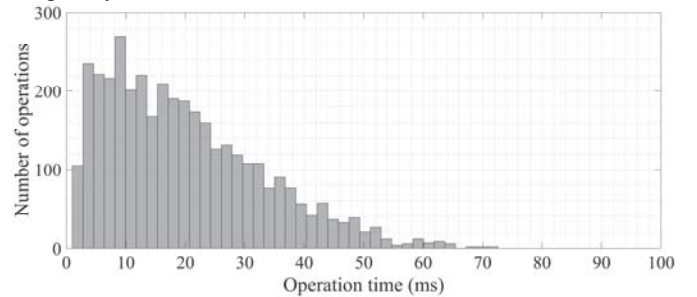
Fig. 14. Histogram of relay operation times for the network of Fig. 7 (*Case B*)

3) Case C

A first analysis is carried out with switch S1 open and switches S2 and S3 closed in the network of Fig. 8. In this configuration, feeder A is meshed and includes only cable lines. The analysis carried out by using the equivalent circuit suggests a filter centered at 0.5 kHz and with a bandwidth of 0.6 kHz. The lower frequencies than in the previous cases are due to the larger capacitances of the underground cables with

respect to overhead lines. As a result, a time window of 5 ms is applied to consider at least one period of the lowest transient frequency. Since the time window in this case is 5 ms, which corresponds to 41 points for f_s = 8 kHz, it might seem that the zero-padding process is not needed since the DFT frequency step f_{step} would be 195.1 Hz (for case A it was 125 Hz after padding). However, with respect to the f_0 used in this case, f_{step} is 39% of f_0, which is a considerably high value. By zero-padding the signal length is increased to 256 points, for which f_{step} = 31.25 Hz, corresponding to 6.25% of f_0.

A series of 500 faults is simulated in lines 8 and 12 varying the fault incidence angle over one power frequency period, the fault resistance between 0 and 400 Ω and the fault location along the line. The main results are reported in Table IV.

TABLE IV
PROTECTION ALGORITHM CHARACTERISTICS AND MAIN RESULTS FOR THE MV NETWORK OF FIG. 8 (*CASE C*) WITH SWITCHES S1 OPEN AND S2 AND S3 CLOSED

Filter f_0/BW (kHz)	0.5/0.6	
t_{win} (ms)	5.0	
$\theta_{min} - \theta_{max}$	190° – 315°	
$v_{0,min}$ (kV)	1.5	
$i_{0,min}$ (A)	0.5	
Faulted line	**Line 8**	**Line 12**
Failures to trip	0.00%	0.00%
Unnecessary trips	0.00%	0.00%

For the Monte Carlo analysis[1] the characteristics of the protection system are the same reported in Table IV. The results show a 0.20% failure to trip rate and a 0.40% unnecessary trip rate. The total mis-operation rate is 0.40% (all the cases in which a failure to trip is verified, are also cases in which an unnecessary trip is registered). The minimum peak values for v_0 and i_0 during the fault are 7.55 kV and 1.70 A, respectively. The results obtained for different operation zones are summarized in Table V.

TABLE V
MONTE CARLO RESULTS FOR DIFFERENT OPERATION ZONES (*CASE C*)

$\theta_{min} - \theta_{max}$	**Failures to trip**	**Unnecessary trips**
180° - 360°	0.20%	0.85%
190° - 315°	0.20%	0.40%
180° - 325°	0.20%	0.60%
200° - 305°	1.35%	0.20%

Fig. 15 shows the histogram of the operation times. The delay introduced by relay processing is considered equal to

[1] As no load is connected between them, both lines 4 and 5 are protected by relays 4A and 5B. When a fault occurs at any point of these lines, the earth-mode current that flows through relay 4A is rather low with a very high transient dominant frequency, since values L_{eq} and C_{eq} are low as there are no other feeders connected to bus A and the relay 4A is close to the substation transformer. On the other hand, relay 4A does not need to be directional and operates whenever the measured current i_0 exceeds the threshold and the permissive signal from 5B is received. The remaining setting parameters, as the time window, are equal to those of the other relays.

5.93 ms. Indeed, the resulting operation times are larger than those of Fig. 13 and Fig. 14, but they do not exceed 100 ms.
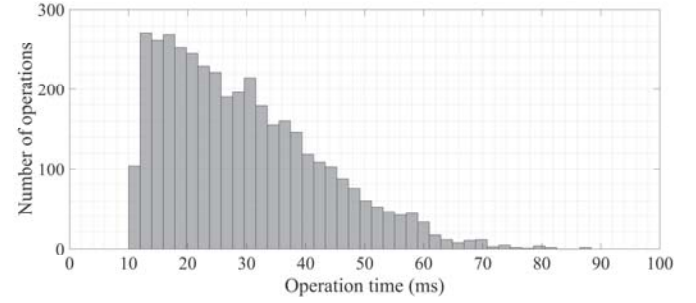

Fig. 15. Histogram of relay operation times. Feeder A of the network of Fig. 8

The second analysis is carried out with all the switches closed. It is worth analyzing the fault within line 3, as the earth mode current at the two-line ends has different behavior. Indeed, for such a fault, relay 3A will sense the current fed only by bus A through cable lines, while relay 3B will measure the current fed only by bus B through overhead lines. These differences are illustrated by Fig. 16 that compares the earth-mode currents at both ends of line 3 when a fault occurs at 10.2 ms in the middle of phase A with a 3 Ω fault resistance.
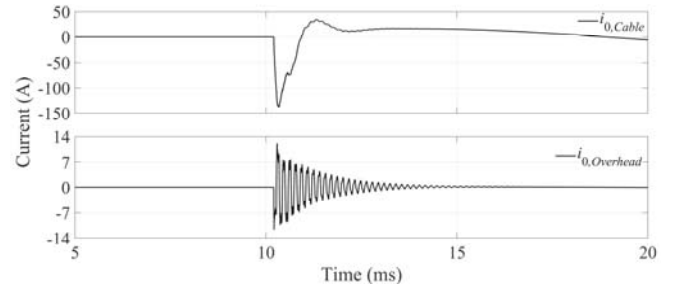

Fig. 16. Earth-mode currents measured at both ends of line 3 due to a fault in the middle of phase A.

The large earth-mode current measured by relay 3A at the cable feeder side (the peak is about ten times that measured by relay 3B, i.e. the relay at the overhead line feeder side) is due to the lower zero-sequence impedance of cables.

The analysis carried out by using the equivalent circuit for these faults indicates the implementation of a filter in the relays of feeder B centered at 6 kHz and with a bandwidth of 3 kHz. These relays need a sampling frequency higher than 8 kHz, which is however appropriate for the relays in feeder A. As in *Case B*, for the sake of the protection algorithm validation, a sampling frequency of 20 kHz is used for the relays of feeder B.

A series of 500 faults is simulated varying the fault incidence angle over one power frequency period, the fault resistance between 0 and 400 Ω and the fault location along the line. The main results are reported in Table VI and show a 0.20% failure to trip rate and a 0.20% unnecessary trip rate. The total mis-operation rate is 0.20% (the fault that leads to a failure to trip is the same that leads to the unnecessary trip).

TABLE VI
PROTECTION ALGORITHM CHARACTERISTICS AND MAIN RESULTS FOR THE
MV NETWORK OF FIG. 8 (*CASE C*) WITH SWITCHES S1, S2 AND S3 CLOSED

Relays of feeder A (cable lines)	**Filter f_0/BW (kHz)**	0.5/0.6
	t_{win} **(ms)**	5.0
	$\theta_{min} - \theta_{max}$	180° – 315°
	f_s **(kHz)**	8
	$v_{0,min}$ **(kV)**	1.5
	$i_{0,min}$ **(A)**	0.5
Relays of feeder B (overhead lines)	**Filter f_0/BW (kHz)**	6.0/3.0
	t_{win} **(ms)**	0.5
	$\theta_{min} - \theta_{max}$	170° – 350°
	f_s **(kHz)**	20
	$v_{0,min}$ **(kV)**	1.5
	$i_{0,min}$ **(A)**	0.5
Faulted line	**Line 3**	
Unnecessary trips	0.20%	
Failures to trip	0.20%	

4) OPAL-RT Test results

To further illustrate the applicability of the protection algorithm, some results obtained by performing real-time simulations are presented. The network of Fig. 8 is considered, with switches S1 open and S2 and S3 closed. The power system and the protection algorithm are both implemented in an Opal-5600 real-time simulator. A PI-equivalent model is used to represent the lines. Indeed, the minimum time step attainable by the simulator is 20 µs, where the frequency dependent model or the constant parameter model would require time steps of less than one microsecond due to the short length of the cables in the network. Moreover, to avoid overruns during the simulation that could lead to inaccurate results, a time step of 62.5 µs is used. A fault is simulated in the middle of line 8 at *t*=10 s with a 10 Ω fault resistance. The communication delays are also considered. In Fig. 17 and Fig. 18 the phase and zero-sequence currents measured at both ends of line 8 and the trip signals are reported. The protection operates properly, opening only the breakers at both sides of the faulted line. When the fault occurs the current measured at both ends of the faulted phase flow in the same direction as happens with phase A in Fig. 17. For the healthy phases instead, one of the ends will see the current flowing into the line, and the other end will see the current flowing out of the line, thus in opposite directions, as happens with phases B and C.
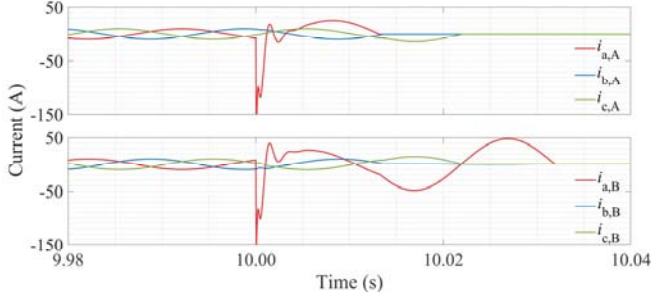

Fig. 17. Phase currents measured at both ends of Line 8 due to a fault in the middle of phase A (the positive direction of the current is from the bus to the line for each relay).
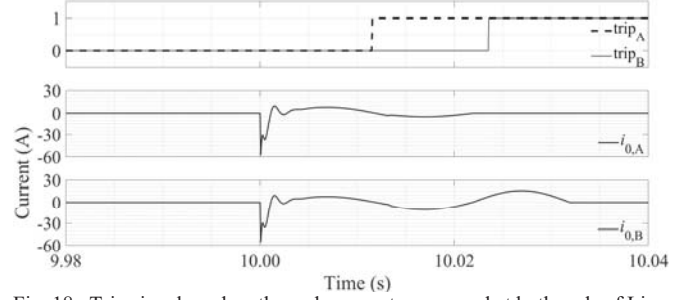

Fig. 18. Trip signals and earth-mode currents measured at both ends of Line 8 due to a fault in the middle of phase A

The main significance of carrying out the real-time simulation is that it demonstrates that the algorithm can perform all the required calculations (filtering, zero-padding, DFT, etc.) in operational times.

IV. CONCLUSIONS

A transient-based protection algorithm for earth fault protection of meshed unearthed MV networks is proposed. The protection system is based on directional relays which implement a transient fault detection algorithm. The algorithm determines the directionality of the fault by calculating the angle between the zero-sequence voltage and current phasors estimated at the dominant frequency of the fault-originated transient. The implementation of a Butterworth filter and a zero-padding process to the input signals enhances the protection performance.

The protection performances are assessed by means of a simulation tool that interfaces EMTP-RV with Matlab. Different MV meshed networks, varying topology, and line configurations, considering unbalanced loads and lines, as well as overhead and underground lines, are considered. The effects of the limits of the communication network on the protection system operation of the protection system have been evaluated. To analyze the behavior of the protection system for different cases, a Monte Carlo method has been used, varying fault resistance, fault incidence angle and fault location within the network. The results support the driving motivation, namely that the protection algorithm is not significantly influenced by the typical factors that might affect the performance of transient methods, i.e. line unbalance, faults at the zero-crossing voltage, and the presence of underground cables.

The communication latencies were also considered. The protection system assessment for the modified IEEE-14 bus overhead line network results in a 0.55% failure to trip rate and a 0.50% unnecessary trip rate when the lines are 3 km long, and a 5.95% failure to trip rate and a 3.00% unnecessary trip rate when the lines are 0.5 km long. The analysis for the cable line feeder of the Cigré network results in a 0.20% failure-to-trip rate and a 0.40% unnecessary trip rate. An analysis varying the operation zones was also carried out. The results obtained do not change considerably when the maximum and minimum angles of the operation zone are

varied within ±10°.

The maximum operation times in all cases in which the protection operates correctly do not exceed 100 ms even in the worst conditions of communication latency.

Opal-RT real time environment has been also used to further illustrate the applicability of the protection approach.

The performances of the protection algorithm depend on the range of variation of the expected dominant transient frequencies, which in turn depends on the network characteristics, mainly on the equivalent capacitance and inductance. As the network includes additional feeders and longer lines, the dominant transient frequencies decrease. For the network with 3-km long overhead lines, a sampling frequency of 8 kHz, attainable by modern relays, is adequate. For the same network, with lines having length of 0.5 km, a higher sampling frequency is required. This limitation affects all the transient-based protection algorithms that use a DFT approach to calculate the dominant transient frequency. As cable networks have large capacitances, the expected dominant frequencies are relatively low and such a limitation is less significant.

Although the need to install two relays per line to isolate only the faulted branch makes the proposed solution more costly, this requirement is needed to fully exploit the benefits of the meshed network configuration. The protection system is proven to be effective mainly for cable line and large overhead line networks.

REFERENCES

[1] Z. Liu, C. Su, H. K. Hoidalen, and Z. Chen, "A Multiagent System-Based Protection and Control Scheme for Distribution System with Distributed-Generation Integration," *IEEE Trans. Power Deliv.*, vol. 32, no. 1, pp. 536–545, 2017.

[2] A. H. Osman, M. S. Hassan, and M. Sulaiman, "Communication-based adaptive protection for distribution systems penetrated with distributed generators," *Electr. Power Components Syst.*, vol. 43, no. 5, pp. 556–565, 2015.

[3] A. Capasso, R. Calone, R. Lama, S. Lauria, and A. Santopaolo, "Ground Fault Protection in ENEL Distribuzione's Experimental MV Loop Line," in *12th IET International Conference on Developments in Power System Protection (DPSP 2014)*, Copenhagen, Denmark, 2014.

[4] W. Wang, S. Jazebi, F. De León, and Z. Li, "Looping Radial Distribution Systems Using Superconducting Fault Current Limiters: Feasibility and Economic Analysis," *IEEE Trans. Power Syst.*, vol. 33, no. 3, pp. 2486–2495, 2017.

[5] G. Celli, F. Pilo, G. Pisano, R. Cicoria, and A. Iaria, "Meshed vs. radial MV distribution network in presence of large amount of DG," in *IEEE PES Power Systems Conference and Exposition.*, 2004, pp. 1357–1362.

[6] J. C. Kim, S. M. Cho, and H. S. Shin, "Advanced power distribution system configuration for smart grid," *IEEE Trans. Smart Grid*, vol. 4, no. 1, pp. 353–358, 2013.

[7] T. H. Chen, W. T. Huang, J. C. Gu, G. C. Pu, Y. F. Hsu, and T. Y. Guo, "Feasibility study of upgrading primary feeders from radial and open-loop to normally closed-loop arrangement," *IEEE Trans. Power Syst.*, vol. 19, no. 3, pp. 1308–1316, 2004.

[8] M. Lehtonen, R. J. Millar, and C. J. Kim, "The Impact of the Distribution Network Type and Configuration on the Transient Behavior of the Fault and Neutral Points during Earth Faults," in *International Conference on Power Systems Transients*, Delft, Netherlands, 2011.

[9] K. Pandakov, H. K. Høidalen, and J. I. Marvik, "Misoperation analysis of steady-state and transient methods on earth fault locating in compensated distribution networks," *Sustain. Energy, Grids Networks*, vol. 15, pp. 34–42, 2018.

[10] S. Hänninen and M. Lehtonen, "Characteristics of earth faults in electrical distribution networks with high impedance earthing," *Electr. Power Syst. Res.*, vol. 44, no. 3, pp. 155–161, 1998.

[11] Institute of Electrical and Electronics Engineers, "IEEE Std. 1547-2018. Standard for Interconnection and Interoperability of Distributed Energy Resources with Associated Electric Power Systems Interfaces," *IEEE Std 1547-2018 (Revision of IEEE Std 1547-2003)*. 2018.

[12] T. Henriksen, "Faulty feeder identification in high impedance grounded network using charge-voltage relationship," *Electr. Power Syst. Res.*, vol. 81, no. 9, pp. 1832–1839, 2011.

[13] M. F. Abdel-fattah and M. Lehtonen, "A New Transient Impedance-Based Algorithm for Earth Fault Detection in Medium Voltage Networks," in *International Conference on Power Systems Transients*, 2009.

[14] M. F. Abdel-Fattah and M. Lehtonen, "Transient algorithm based on earth capacitance estimation for earth-fault detection in medium-voltage networks," *IET Gener. Transm. Distrib.*, vol. 6, no. 2, pp. 161–166, 2012.

[15] M. F. Abdel-Fattah and M. Lehtonen, "A transient fault detection technique with varying fault detection window of earth modes in unearthed MV systems," in *6th International Conference - Power Quality and Supply Reliability*, 2008.

[16] P. Balcerek, M. Fulczyk, J. Izykowski, E. Rosolowski, and P. Pierz, "Centralized substation level protection for determination of faulty feeder in distribution network," in *IEEE Power and Energy Society General Meeting*, San Diego, CA, USA, 2012.

[17] J. L. Blackburn and T. J. Domin, *Protective Relay Principles*. CRC Press, 2006.

[18] J. D. Rios Penaloza, A. Borghetti, F. Napolitano, F. Tossani, and C. A. Nucci, "Performance Analysis of a Communication-Supported Earth Fault Protection System of Medium Voltage Loop and Meshed Networks," in *18th EEEIC Environment and Electrical Engineering International Conference*, Palermo, Italy, Italy, 2018, pp. 1314–1319.

[19] M. J. Thompson and A. Somani, "A tutorial on calculating source impedance ratios for determining line length," in *68th Annual Conference for Protective Relay Engineers*, College Station, TX, USA, 2015, pp. 833–841.

[20] J. Arrillaga and N. R. Watson, *Power system harmonics*. John Wiley & Sons Ltd., 2003.

[21] R. Moxley and K. Fodero, "High-speed distribution protection made easy: Communications-assisted protection schemes for distribution applications," in *58th Annual Conference for Protective Relay Engineers*, College Station, TX, USA, USA, 2005.

[22] E. O. Schweitzer, D. Finney, and M. V. Mynam, "Applying radio communication in distribution generation teleprotection schemes," in *65th Annual Conference for Protective Relay Engineers*, College Station, TX, USA, 2012, pp. 310–320.

[23] S. V Achanta, B. Macleod, E. Sagen, H. Loehner, and S. E. Laboratories, "Apply Radios to Improve the Operation of Electrical Protection," *SEL J. Reliab. Power*, vol. 1, no. 2, 2010.

[24] H. J. Altuve, K. Zimmerman, and D. Tziouvaras, "Maximizing line protection reliability, speed, and sensitivity," in *69th Annual Conference for Protective Relay Engineers*, College Station, TX, USA, 2016, pp. 1–28.

[25] Western Electricity Coordinating Council (WECC) - Telecommunications and Relay Work Groups, "Communications Systems Performance Guide for Electric Protection Systems," 2013. [Online]. Available: https://www.wecc.org/Reliability/Communication System Performance Guide for Electric Protection Systems.pdf.

[26] R. Bottura, D. Babazadeh, K. Zhu, A. Borghetti, L. Nordstrom, and C. A. Nucci, "SITL and HLA co-simulation platforms: Tools for analysis of the integrated ICT and electric power system," in *IEEE 2013 EuroCon*, 2013, pp. 918–925.

[27] CIGRE Working Group C4.605, "Benchmark Systems for Network Integration of Renewable and Distributed Energy Resources," CIGRE, Paris, France, Tech. Rep. C6.04.02, 2014.

Juan Diego Rios Penaloza (S'18) started his studies in the Universidad Mayor de San Simón, Cochabamba, Bolivia, and then transferred to the University of Bologna, Italy, where he received the B.Sc. and M.Sc. (Hons.) degrees in electrical engineering in 2012 and 2014, respectively. He is

currently a Ph.D. student in electrical engineering at the University of Bologna. His research interests include the analysis of power systems transients, power systems protection, integration of distributed energy resources in the distribution network and microgrids.

Alberto Borghetti (M'97–SM'03–F'15) received the Laurea degree in electrical engineering (with honors) from the University of Bologna, Bologna, Italy, in 1992. Since then he has been working with the power system group of the same University, where is now a Professor of Electrical Power Systems. His research and teaching activities are in the areas of power system analysis, power system restoration after blackout, electromagnetic transients, optimal generation scheduling, and distribution system operation. He has received the Int. Conf. on Lightning Protection (ICLP) Scientific Committee Award in 2016 and the 2018 CIGRE Technical Council Award for SC C4 (System Technical Performance). From 2010 to 2017 he served as an Editor of *IEEE Trans. on Smart Grid*. Currently he is serving as an Editor of *IEEE Trans. on Power Systems*, Associate Editor of *MPCE*, and Editor-in-Chief of *Electrical Engineering – Archiv fur Elektrotechnik*.

Fabio Napolitano (M'16-SM'17) is an Associate Professor at the Department of Electrical, Electronic and Information Engineering of the University of Bologna, Italy. From the same University, he received the M.S. degree (with hons.) in electrical engineering in 2003 and the Ph.D. degree in electrical engineering in 2009. His research interests are the analysis of power systems transients, in particular those due to indirect lightning strokes, and lightning protection systems. He is member of the Technical Committee 81 of CEI and Associate Editor of *Electrical Engineering – Archiv fur Elektrotechnik*.

Fabio Tossani (S'15-M'16) received the B.S. (Hons.), M.S. (Hons.) and Ph.D. degrees in electrical engineering from the University of Bologna, Italy, in 2010, 2012 and 2016, respectively. He is a junior Assistant Professor of the Power Systems Laboratory of the Department of Electrical, Electronic and Information Engineering "Guglielmo Marconi", University of Bologna. His research interests are power system transients, lightning electromagnetic pulse interaction with electrical networks, power systems protection and the integration of renewables in power distribution networks. He is Assistant Editor of the *Electric Power Systems Research* and Associate Editor of *Electrical Engineering – Archiv fur Elektrotechnik*.

Carlo Alberto Nucci (M'91–SM'02–F'07) graduated with honors in electrical engineering from the University of Bologna, Bologna, Italy, in 1982. He is a Full Professor and Head of the Power Systems Laboratory of the Department of Electrical, Electronic and Information Engineering Guglielmo Marconi, University of Bologna. He is an author or coauthor of over 370 scientific papers published in peer-reviewed journals or in proceedings of international conferences. Prof. Nucci is a Fellow of the International Council on Large Electric Systems (CIGRE), of which he is also an honorary member, and has received some best paper/technical international awards, including the CIGRE Technical Committee Award and the ICLP Golde Award. From January 2006 to September 2012, he served as Chairman of the Cigre Study Committee C4 System Technical Performance. He has served as IEEE PES Region 8 Rep in 2009 and 2010. Since January 2010, he has served as Editor-in-Chief of the Electric Power Systems Research journal (Elsevier). He has served as the President of the Italian Group of the University Professors of Electrical Power Systems (GUSEE) from 2012 to 2015. Prof. Nucci is Doctor Honoris Causa of the University Politehnica of Bucharest and a member of the Academy of Science of the Institute of Bologna.